

PSP-coordinated nickel(II) complexes as Kumada coupling catalysts

Franziska Flecken^a, Toni Grell^b and Schirin Hanf^{a}*

^a Institute for Inorganic Chemistry, Karlsruhe Institute of Technology, Engesserstr. 15, 76131 Karlsruhe, Germany, schirin.hanf@kit.edu

^b Dipartimento di Chimica, Università degli Studi di Milano, Via Camillo Golgi 19, 20131 Milano, Italy.

Abstract

Phosphine-coordinated nickel complexes are well-known catalysts in Kumada-Tamao-Corriu coupling reactions. In this context, often PCP-type phosphines ($R_2P(C_2H_4)PR_2$ or $R_2P(C_3H_6)PR_2$) have been studied, while sulphur-containing analogues, such as PSP-type ligands (R_2PSPR_2), have been largely overlooked. In this work we present the synthesis of PSP-based nickel complexes of the form $[NiHal_2(PSP)]$, $PSP = Ph_2PSPH_2$, $Hal = Br$ (**1**), I (**2**) *via* a facile one-pot reaction of the free ligand and the respective nickel halides. Attempts to synthesise the Cl analogue results in the formation of a multinuclear nickel complex, such as $[Ni_2(Ph_2PSS)_2(Ph_2PS)(Ph_2P)]$, in which Ph_2PSS^- , Ph_2PS^- and Ph_2P^- ligands coordinate to the Ni-centres, which were found to form *via* ligand rearrangement processes of the parent PSP ligand. Complexes **1** and **2** were used as catalysts in Kumada coupling reactions and revealed a great potential for the coupling of sterically

demanding substrates, whereby no sulphur poisoning induced by the ligand backbone could be identified.

Introduction

The application of phosphine-stabilised nickel complexes in homogeneous catalysis attracts a great deal of attention, especially with regard to a sustainable catalyst development and the potential to replace noble metal-based catalysts, such as palladium complexes.¹⁻³ One important reaction in this context is the Kumada-Tamao-Corriu coupling of aryl halides with Grignard reagents to form high value C–C coupled products, which find wide applications in the fields of pharmaceuticals, agrochemicals or fine chemicals.⁴ Initially, bidentate PCP-type based nickel halide complexes [PCP = dppe (C = C₂H₄), dppp (C = C₃H₆), dppb (C = C₄H₈)] were applied in the Kumada coupling, whereby a clear impact of the ligand backbone on the catalytical outcome was observed.^{5,6}

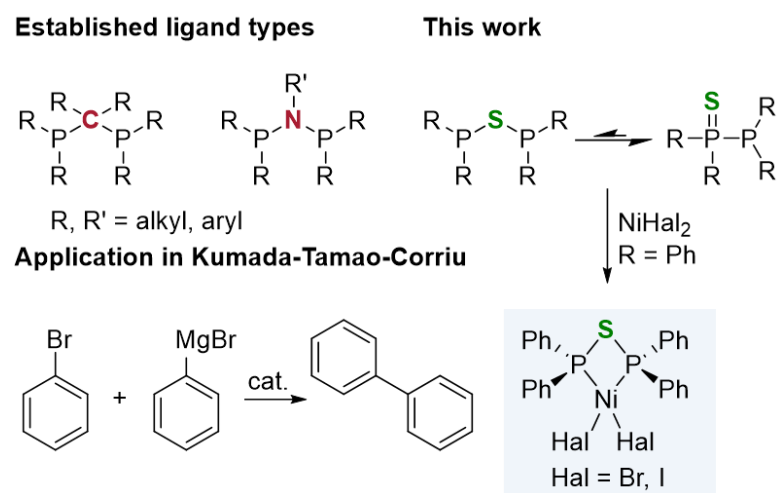


Figure 1. Conventional bidentate ligands (PCP- and PNP-based) applied in the Kumada-Tamao-Corriu coupling and their corresponding PSP counterparts and corresponding nickel complexes.

Despite the fact, that the modification of the PCP-type ligand *via* the carbon-based bridging unit has been investigated, further variations, for example the incorporation of another heteroatom,

such as sulphur, in the ligand backbone, has largely been overlooked. This might be due to the fact that sulphur compounds are usually considered to be catalyst poisons in many cases, which undermines their potential.^{7, 8} A second reason might be that the simplest PSP-type ligand, Ph₂P–S–PPh₂, obtains an interesting tautomeric equilibrium, which is shifted to the PPS-form (Ph₂P(=S)–PPh₂) under ambient conditions (Figure 1). However, PSP-based compounds can be stabilised, when strongly electron withdrawing groups are bound to the phosphorus atom,⁹ or in the presence of transition metals *via* the formation of so-called coordination-stabilised tautomers.⁹

10

Despite the vastly under-explored research on PSP-type ligands, a few examples of transition metal complexes have been reported, among which chelate complexes are rare due to the high ring strain in the four-membered ring. Accordingly, only two reports describe the isolation of such PSP-based chelate complexes including one Mo-¹¹ and three Ru-based¹² complexes. More examples exist for the group of dinuclear complexes, while merely one example for Fe⁹ and one for Cr¹³ cover mononuclear complexes with a PPS coordination *via* the P-atom (Figure 2).

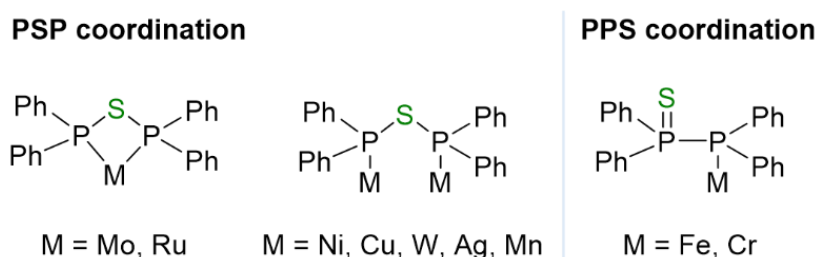


Figure 2. Different coordination modes of the PSP (left) and PPS (right) tautomer of the ligand system. Other ligands on the metal centres are omitted for clarity. Chelate compounds are only known for Mo¹¹ and Ru¹². Isolated dinuclear complexes have been reported for Ni¹⁴, Cu¹⁰, W¹⁵, Ag⁹ and Mn¹⁶, whereas coordination complexes of the PPS-type ligand were reported for Fe⁹ and Cr.¹³

We have recently reported PXP-stabilised trinuclear copper complexes of the form $[\text{Cu}_3(\mu_3\text{-Hal})_2(\mu\text{-PXP})_3]\text{PF}_6$ ($X = \text{O}, \text{S}; \text{Hal} = \text{Cl}, \text{Br}, \text{I}$), which are formed through the conversion of $[\text{Cu}(\text{MeCN})_4]\text{PF}_6$ with $\text{K}(X=)\text{PPh}_2$ ($X = \text{O}$: KPO, $X = \text{S}$: KPS) and HalPPh_2 involving the *in-situ* formation of the PXP ligand. The *in-situ* ligand formation was required to avoid either ligand decomposition reactions, which lead to the isolation of tetraphenyl diphosphine-based Cu(I) complexes in the case of PSP, or the formation of di- or tetranuclear Cu-complexes in the case of POP.

Hereby, a tremendous impact of the ligand backbone on the compounds features was observed, since not only the geometric constitution of the complexes was altered but also the photo-physical properties were affected. By changing the heteroatom within the ligand backbone from oxygen ($\text{Ph}_2\text{P-O-PPh}_2$) to sulphur ($\text{Ph}_2\text{P-S-PPh}_2$), photo-emission could be manipulated by the choice of ligand backbone.¹⁰ Inspired by the great effect of the choice of ligand backbone on the formation of trinuclear copper complexes and their photo-optical properties, the impact of the sulphur-containing ligand backbone is investigated in Ni(II) complexes as coupling catalysts as part of this study. The incorporation of sulphur into the ligand backbone and the therewith involved different electronic and steric properties of the ligand backbone in comparison to conventional PCP-type ligands, should open up new pathways in tuning the activity and selectivity of nickel catalysts.

Results and Discussion

Synthesis and molecular structure of PSP-stabilised nickel complexes

In analogy to the formation of trinuclear PSP-stabilised Cu(I) complexes, initial studies for the isolation of Ni(II)-based compounds, concentrated on the conversion of $[\text{Ni}(\text{MeCN})_4](\text{BF}_4)_2$ in the presence of KPS and HalPPh_2 ($\text{Hal} = \text{Cl}, \text{Br}, \text{I}$). From this reaction the desired complexes $[\text{NiHal}_2(\text{PSP})]$ [$\text{Hal} = \text{Br}$ (**1**), I (**2**)] were isolated for the first time. Interestingly, in both cases the

PSP ligand acts as chelate ligand forming a four membered Ni–P–S–P ring. Alternatively, both complexes could also be successfully synthesized in a direct reaction of PPS with nickel bromide and iodide by refluxing the nickel halides in acetonitrile in presence of the ligand.

Violet crystals of **1** and **2** could be grown from DCM layered with *n*-heptane which could be used for the determination of the solid-state structures by means of single crystal XRD.

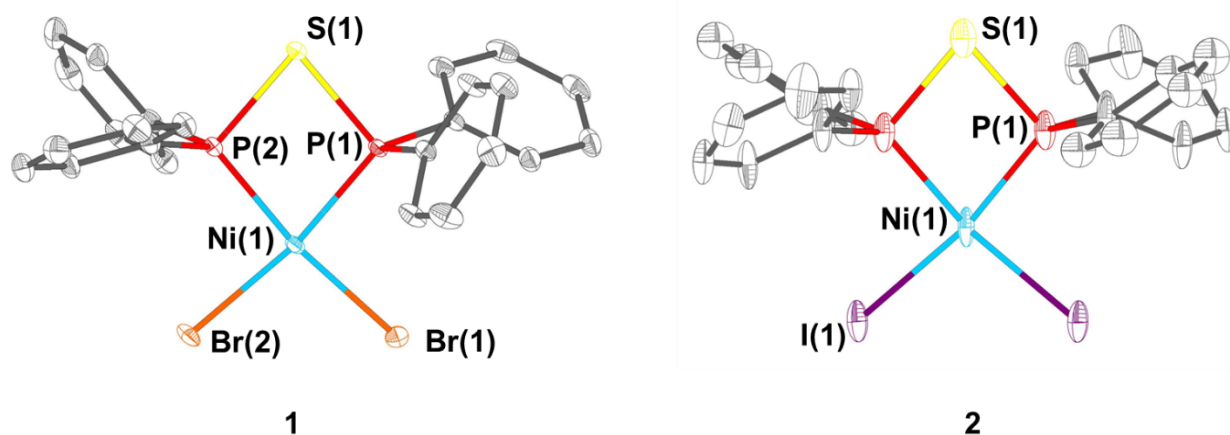


Figure 3. Molecular structures of the $[\text{NiHal}_2(\text{PSP})]$ complexes **1** (Hal = Br) and **2** (Hal = I).

Table 1. Selected bond lengths [Å], angles [°] and structural parameters of **1** and **2** in the solid state.

	$[\text{NiBr}_2(\text{PSP})]$ (1)	$[\text{NiI}_2(\text{PSP})]$ (2)
P–S	2.1146(7)–2.1183(7)	2.117(3)
P–Ni	2.1347(6)–2.1425(6)	2.137(3)
Ni–X	2.3271(4)–2.3370(4)	2.5251(7)
P–C	1.799(2)–1.812(2)	1.814(6)–1.816(7)
X–Ni–X	97.234(13)	100.57(8)
X–Ni–P	91.613(19)–171.07(2)	89.93(7)–167.36(6)
Ni–P–S	99.43(3)–99.80(3)	98.93(10)
P–S–P	80.81(3)	81.51(15)

P–Ni–P	79.80(2)	80.62(13)
Distance Ni–best plane ^a	0.008	0.000
τ'_4 ^b	0.13	0.18

^a The best plane is defined by the two P-atoms of the PSP ligand and two halides; distance to this plane is given in Å; ^b Structural index parameter¹⁷: $\tau'_4 [-] = ((\beta-\alpha)/(360-\theta))+((180-\beta)/(180-\theta))$, β, α : largest valence angles $\beta > \alpha$, θ : tetrahedral angle $\cos^{-1}(-1/3) \sim 109.47$; $\tau'_4 \sim 0$ for square planar and $\tau'_4 \sim 1$ for tetrahedral coordination

Both compounds **1** and **2** show similar structures in the solid-state featuring four-membered, nearly planar chelate rings (Ni–P–S–P) that form the core of the structures. As a result of the larger atomic radius of sulphur compared to carbon and the therewith induced elongated distance between the two phosphorus atoms of the PSP scaffold, the bite angles of **1** and **2** are both around 80° (Table 1) and therefore larger than the one reported for the PCP analogue [NiBr₂(dppm)] (dppm = bis(diphenylphosphino)methane) with 75.95(8)°. ¹⁸ Compared to the P–C–P angle of the PCP-type ligand in [NiBr₂(dppm)] (91.94°), the P–S–P angles (80.81(3)° for **1** and 81.51(15)° for **2**) present a relatively acute backbone. This acute bond angle is a requirement for the formation of the chelate complexes with the PSP ligand which in many other cases is impeded by a high ring strain that instead leads to either the coordination in a monodentate fashion or the coordination of two separate metal atoms.^{11, 19} The P–S–P bond angles for the only hitherto observed chelate-type complexes incorporating PSP-type ligands, are slightly larger with 86.9° for Mo¹¹ and 82.1°–82.46° for the Ru complexes¹². The P–S bonds in **1** (2.1146(7)–2.1183(7) Å) and **2** (2.117(3) Å) are slightly shorter than in the Mo and Ru complexes (2.123(4)–2.145(6) Å) but are in the same range as seen in [Cu₃(μ_3 -Hal)₂(μ -PSP)₃]PF₆ (Hal = Cl, Br, I) with bond lengths of 2.108(3)–

2.120(3) Å.¹⁰ The P–M bond is smaller than the one in Mo and Ru complexes and is therefore in accordance with other bidentate phosphine-Nickel complexes such as [NiBr₂(dppe)] (2.141(1), 2.156(1) Å)²⁰ and [NiBr₂(dppm)] (2.1423(16) Å).¹⁸ As expected, the Ni–I (2.5251(7) Å) is longer than the Ni–Br (2.3271(4)–2.3370(4) Å) bond.

UV/Vis absorption spectra have been recorded for the two colourful complexes (Figure 4). In a DCM solution of **1**, a broad absorption band can be observed at around 510 nm ($\epsilon = 2391 \text{ dm}^3 \text{ mol}^{-1} \text{ cm}^{-1}$) in the visible region, due to the larger ligand field splitting induced by the bromo ligand, while for **2** this absorption band is shifted to lower energies with a maximum at around 564 nm ($\epsilon = 2297 \text{ dm}^3 \text{ mol}^{-1} \text{ cm}^{-1}$). The respective transitions are responsible for the red-violet (**1**) and dark violet (**2**) colorations and can be ascribed to M–L charge transfer transitions.

The quasi square planar coordination of the nickel(II) centre is indicated by the structural index parameters (

Table 1) and explains the diamagnetic nature of the compounds, which is supported by sharp signals in the NMR spectra (³¹P{¹H} NMR: **1**: –17.5 ppm; **2**: –14.5 ppm, Figures S2 and S7). This is against the expectations that the bromide should lead to a higher deshielding of the phosphorus atoms, due to its higher electronegativity compared to iodide which would consequently cause a downfield shift of **1** compared to **2**. Similar observations were made by Fergusson and Heveltdt²¹ for other noble-metal based square-planar [MHal₂(PR₃)₂] (M = Pd, Pt; Hal = Cl, Br, I) complexes, which they attributed to either a polarisation effect or a M → Hal π -backbonding in the order of I > Br > Cl.

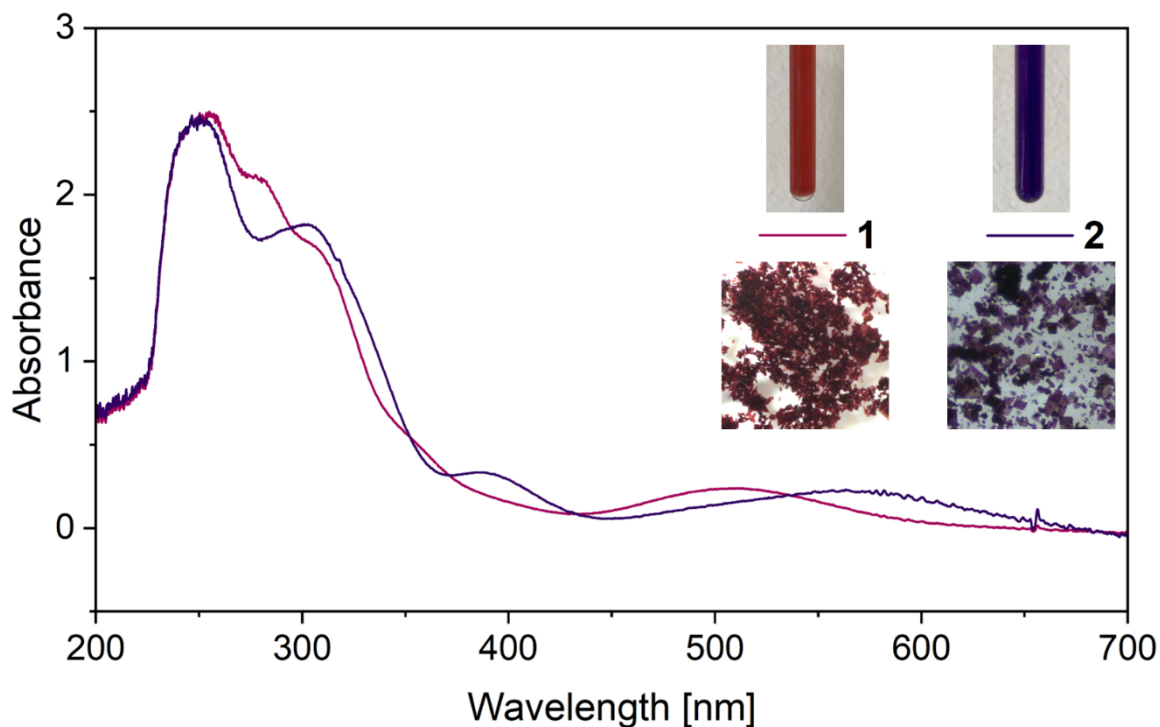


Figure 4. UV/Vis absorption spectra and microscope images of the complexes **1** and **2** in DCM solution ($c = 1 \cdot 10^{-4} \text{ mol L}^{-1}$). Broad maxima in the visible range at 510 nm (**1**) and 564 nm (**2**) are causing the intense red-violet (**1**) and dark-violet (**2**) colours of the compounds.

Attempts were also focused on the isolation of the chloride analogue $[\text{NiCl}_2(\text{PSP})]$. The synthesis was attempted using several methods: *via* the direct reaction of NiCl_2 and the PPS ligand, *via* the conversion of $[\text{Ni}(\text{MeCN})_4](\text{BF}_4)_2$ with the PPS ligand or the ligand precursors KPS and ClPPh_2 , as well as *via* ligand exchange reactions using PPS and $[\text{NiCl}_2(\text{dppe})]$ or $[\text{NiCl}_2(\text{PPh}_3)_2]$. However, none of these synthetic routes lead to the successful isolation of the expected $[\text{NiCl}_2(\text{PSP})]$ complex. Instead, several signals with a strong down-field shift are displayed in the $^{31}\text{P}\{^1\text{H}\}$ NMR spectra, which point towards the formation of new P-containing compounds. This is confirmed by the isolation and characterization of the molecular structure of **3**, namely

$[\text{Ni}_2(\text{Ph}_2\text{PSS})_2(\text{Ph}_2\text{PS})(\text{Ph}_2\text{P})]$, by means of single crystal XRD (Figure 5). Furthermore, reactions of $[\text{Ni}(\text{COD})_2]$ (COD = cycloocta-1,5-diene), as alternative nickel source, with PPS or KPS and ClPPh_2 were attempted. In these cases, either the trinuclear nickel complex **4**, $[\text{Ni}_3(\text{Ph}_2\text{PS})_4(\text{Ph}_2\text{P})_2]$, or the dinuclear nickel complex **5**, $[\text{Ni}_2(\text{Ph}_2\text{PSS})(\text{Ph}_2\text{PS})_2(\text{Ph}_2\text{P})]$, were isolated, in which the nickel(II) atoms are coordinated by Ph_2PSS^- , Ph_2P^- and Ph_2PS^- ligands (Figure 5). Interestingly, in the reaction with $[\text{Ni}(\text{COD})_2]$ an oxidation of Ni(0) to Ni(II) occurred. The formation of Ph_2PSS^- , Ph_2P^- and Ph_2PS^- ligands must be the result of rearrangements of the parent PPS ligand. Ogawa reported similar rearrangements which involved, initiated by UV radiation or radical starters,^{7, 22-24} a homolytic P–P bond cleavage of PPS yielding one $\text{Ph}_2\text{P}(=\text{S})^\bullet$ and one $\text{Ph}_2\text{P}^\bullet$ radical, that could individually recombine to give new compounds. DFT calculations proved the localization of the HOMO mostly at the P(=S)–P unit rather than at the phenyl rings which they suggested to be the major reason for the high reactivity of these compounds.²² We assume, that the coordination of the PSP ligand to nickel facilitates similar bond cleavages which enables rearrangements of the ligand in the case of chloride-containing precursors or Ni(0) precursors resulting in the formation of compounds **3-5**. It should be mentioned that the absence or presence of light did not show an impact on the product formation.

In the multinuclear complexes **3-5**, the Ni(II) atoms are coordinated in a quasi-planar arrangement (Figure 5). A further common feature is the terminal ligands that chelate the one nickel atom involving either two Ph_2PSS^- (**3**), two Ph_2PS^- (**4**) or one Ph_2PSS^- and one Ph_2PS^- ligand (**5**). Furthermore, in all three complexes the nickel atoms are bridged by a combination of one Ph_2P^- ligand and one diametrically opposite Ph_2PS^- ligand leading to five-membered $\text{Ni}_2\text{P}_2\text{S}$ metallacycles. The different coordination modes of the Ph_2PS^- ligand is causing differences in the molecular parameters. In complex **4** and **5**, the internal Ph_2PS^- ligand shows an elongated P–S

bond compared to the one in the terminal Ph_2PS^- ligand, while for the Ni–S bond the opposite is true (Table 2).

In some reactions for the synthesis of **1** and **2**, small amounts of compounds **3-5** could be observed as byproducts. It should be mentioned that UV radiation of complexes **1** and **2** in solution did not initiate any formation of similar multinuclear Ni-compounds (Figure S22).

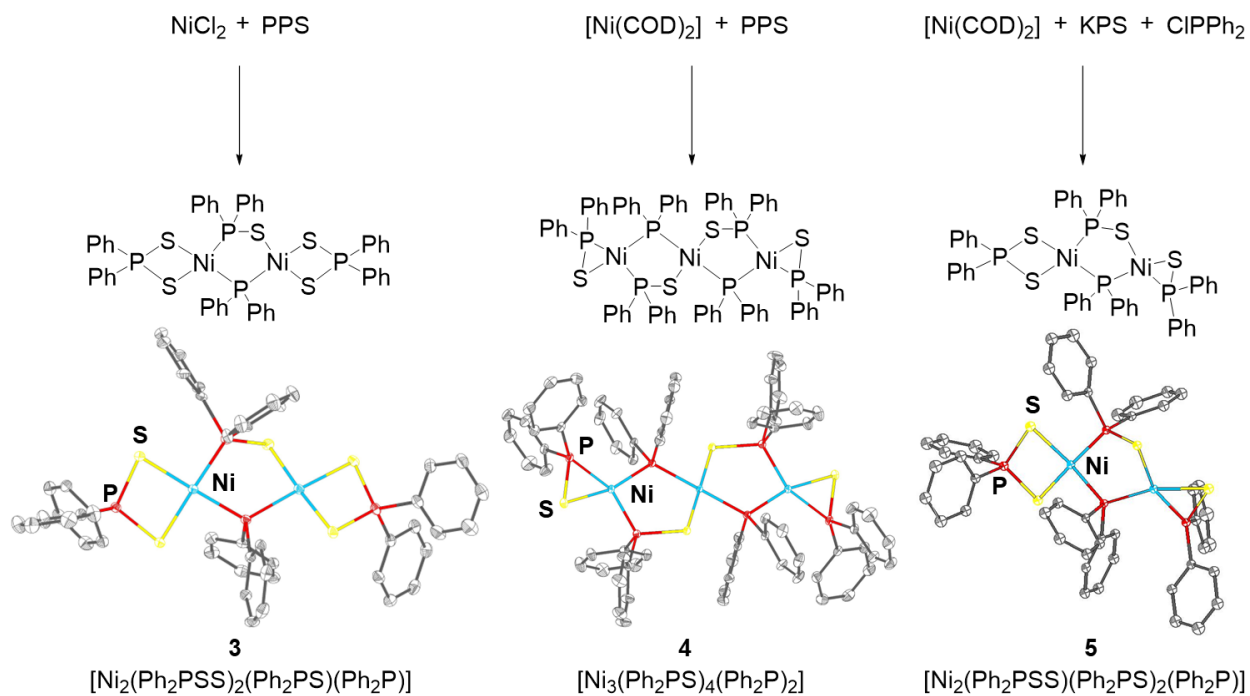


Figure 5. Molecular structures of multinuclear Ni(II) complexes, resulting from the conversion of NiCl_2 and PPS (**3**), $[\text{Ni}(\text{COD})_2]$ and PPS (**4**) and $[\text{Ni}(\text{COD})_2]$ and KPS and ClPPh_2 (**5**). Coordinating ligands Ph_2P^- , Ph_2PS^- and Ph_2PSS^- result from the rearrangement of the PPS ligand.

Table 2. Selected bond lengths [\AA] in the different ligands (Ph_2PS^- , Ph_2PSS^- and Ph_2P^-) of the multinuclear Ni complexes **3**, **4**, **5**.

Compound	Ligand	P–S	P–Ni	S–Ni
3	Ph_2PS_2^-	1.9949(11)–	2.8200(8)–	2.2311(9)–
		2.0176(10)	2.8385(8) ^a	2.2826(8)
5	Ph_2PS_2^-	2.0084(10)–	2.8208(7) ^a	2.2428(7)–
		2.0086(10)		2.2664(8)
3	Ph_2PS^- (intern.)	2.0357(10)–	2.1448(9)–	2.1784(9)–
		2.0394(10)	2.1467(8)	2.1900(9)
4	Ph_2PS^- (term.)	2.0246(7)	2.1477(5)	2.2102(5)
4	Ph_2PS^- (intern.)	2.0616(6)	2.1353(5)	2.1739(4)
5	Ph_2PS^- (term.)	2.0064(10)	2.0962(7)	2.2498(7)
5	Ph_2PS^- (intern.)	2.0421(9)	2.1642(7)	2.2078(7)
3	Ph_2P^-	-	2.1999(8)–	-
			2.2045(8)	
4	Ph_2P^-	-	2.1844(5);	-
			2.2711(4)	
5	Ph_2P^-	-	2.1665(7);	-
			2.1915(7)	

^a Atom–Atom distance, no direct bond

The NMR spectra of compounds **3-5** agree with the molecular structures obtained from X-ray diffraction. Based on the structural index parameters¹⁷ of **3-5**, a nearly square planar coordination mode can be confirmed for nickel(II) in all complexes which is less ideal for **4** and **5** in comparison to complex **3** (Table 3). The comparison of the distances of the Ni(II) atoms to the best plane, defined by the four coordinating P- and S- atoms, indicates the highest deviation from an ideal planarity for **4**. Consequently, a higher paramagnetic character can be assumed for **4** which is visible in the $^{31}\text{P}\{^1\text{H}\}$ NMR spectrum, since **4** shows very broad signals.

Table 3. Classification of the coordination environment in **3-5** based on the distance of the Ni(II) atoms to the best plane [Å] and on the structural index parameter τ'_4 [-]

	3	4	5
Distance Ni–best plane ^a	0.003–0.079	0.000–0.099	0.001–0.056
τ'_4 ^b	0.03–0.10	0.000–0.24	0.13–0.27

^a The best plane is defined by the four coordinating P and S atoms of the ligands; ^b Structural index parameter¹⁷: τ'_4 [-] = $((\beta-\alpha)/(360-\theta))+((180-\beta)/(180-\theta))$, β, α : largest valence angles $\beta > \alpha$, θ : tetrahedral angle $\cos^{-1}(-1/3) \sim 109.47^\circ$; $\tau'_4 \sim 0$ for square planar and $\tau'_4 \sim 1$ for tetrahedral coordination

Compounds **3** and **5** exhibit $^{31}\text{P}\{^1\text{H}\}$ NMR spectra with distinct signals, whereby $^2J_{\text{PP}}$ couplings > 30 Hz and $^3J_{\text{PP}}$ couplings < 10 Hz can be identified (Figure 6, naming scheme shown in the ESI, Figure S11). The signal corresponding to the Ph_2PSS^- ligand can be found in the region of 73 ppm (**3**: 72.7 (P_d) ppm, **4**: 72.0 (P_a) ppm; **5**: 73.0 (P_a) ppm). The different coordination environments in terminal and internal Ph_2PS^- ligands cause a drastic shift in the $^{31}\text{P}\{^1\text{H}\}$ NMR spectra. The terminal Ph_2PS^- can be found at chemical shifts of around 30 ppm (**3**: no terminal Ph_2PS^- ; **5**: 31.1 (P_d) ppm) while signals at around 90 ppm can be related to internal Ph_2PS^- ligands (**3**: 92.0 (P_b) ppm; **5**: 90.1 (P_b) ppm). Signals at around 60 ppm can be attributed to the Ph_2P^- ligand (**3**: 60.4 (P_c) ppm; **5**: 56.3 (P_c) ppm).

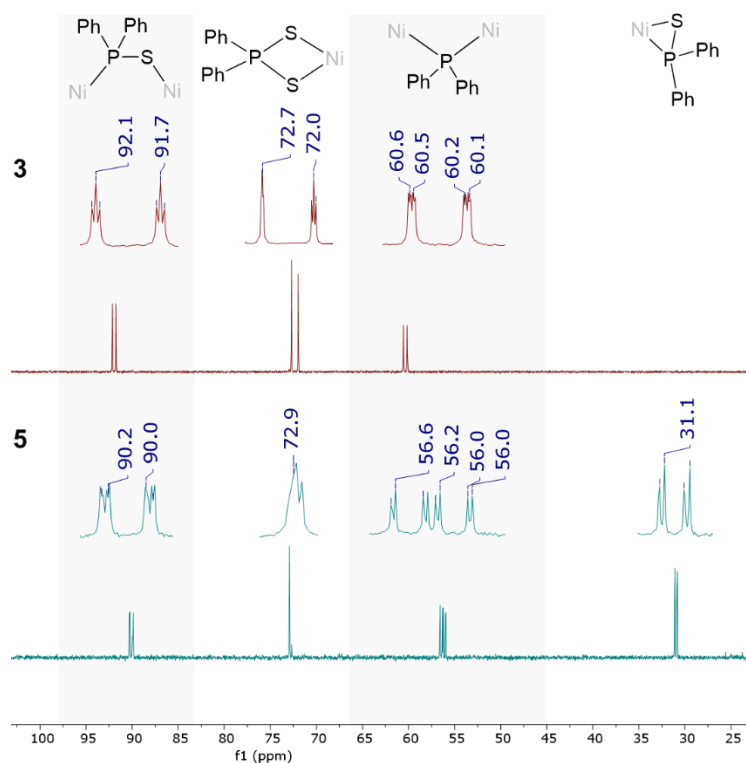


Figure 6. $^{31}\text{P}\{^1\text{H}\}$ NMR (298 K, CD_2Cl_2 , 162 MHz) spectra of **3** and **5**.

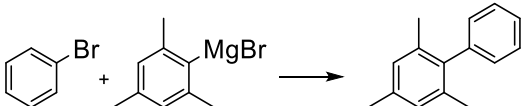
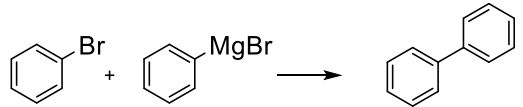
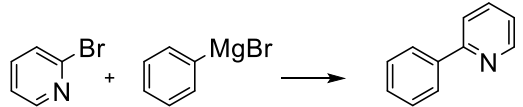
Catalytic application of **1** and **2** in Kumada coupling reactions

Bidentate phosphine-based transition metal complexes are well-established catalysts. Among these nickel-based complexes are leading examples for Kumada-Tamao-Corriu coupling reactions.⁶ Thus, the application of **1** and **2** in such reactions was attempted with the primary aim to investigate the influence of the sulphur backbone in comparison to well-known PCP-type ligand-based nickel complexes.^{5, 6, 25} To the best of our knowledge the application of PSP-type ligands in catalysis has not yet been described in literature. Therefore, $\text{C}(sp^2)\text{-C}(sp^2)$ couplings were conducted in THF, toluene and benzene using **1**, **2** and $[\text{NiBr}_2(\text{dppe})]$ as reference catalyst. Firstly, the successful conversions of the aryl halides prove that PSP-based systems can be applied as efficient catalysts for Kumada coupling reactions, as no indication of catalyst poisoning by the sulphur ligand backbone can be observed. This is in agreement with a study of Li and coworker who applied a

phosphine sulphide [(*t*Bu)₂PSH] ligand in nickel complexes for Kumada-Tamao-Corrio couplings of aryl chlorides with aryl Grignard reagents.⁸

Interestingly, in our case a tremendous impact of the solvent on the catalytic outcome was identified for all three catalysts (Table 4). For example, when [NiBr₂(dppe)] was used, a conversion of 74% of bromobenzene can be achieved in the reaction with MesMgBr in THF, while only minimal conversion of the same substrates was obtained in benzene or toluene after 24 h. Contrary, by using the PSP-based complexes **1** and **2**, the conversion is increased in toluene compared to benzene and THF. This can be explained by the different solubilities and reactivities of the metal complexes in solution. Whereas the reference catalyst [NiBr₂(dppe)] shows a good solubility in THF, without any detectable ligand dissociation, the solubility in benzene and toluene has proven to be very low by NMR spectroscopic analyses of the complex (Figure S25), which leads to a severe drop in catalytic activity. In contrast, **1** exhibits a good solubility in benzene, whereas no dissolved species can be detected in the ³¹P{¹H} NMR spectrum of **1** in toluene (Figure S23). Interestingly, if complex **1** is dissolved in THF a dark red-violet solution becomes obvious, which shows signals in the ³¹P{¹H} NMR spectrum that can be assigned to the free PPS ligand ($\delta = 43.9$ ppm, d, P=S, $^1J_{PP} = 247.3$ Hz; -14.0 ppm, d, PPh₂, $^1J_{PP} = 247.3$ Hz). Thus, it can be concluded that the PSP ligand of **1** is partially liberated in the presence of a coordinating solvent, such as THF, resulting in free coordination sites. In the ³¹P{¹H} spectrum of **2**, recorded in THF, no free PPS ligand can be observed (Figure S24). However, in addition to the signal of **2**, other signals can be detected, which point towards the formation of new nickel complexes with chemically non-equivalent phosphorus atoms. Two of those signals are also present in benzene, while toluene does only show the signal which can be assigned to **2**.

Table 4. Catalytic results using **1**, **2** or [NiBr₂(dppe)] (ref) as catalysts in the coupling reaction of aryl halides and Grignard reagents. Reaction conditions: aryl halide (1 eq.) and Grignard reagent (1 eq.) are reacted in the named solvents for 20 h at room temperature. Conversions of aryl halides were determined by GC-MS using *n*-decane as internal standard.

	Conversion [%]			Selectivity [%]			
	THF	C ₆ D ₆	Tol.	THF	C ₆ D ₆	Tol.	
	1	45	26	63	100	100	100
	2	48	14	52	100	100	100
	ref	74	0	14	100	-	100
	1	39	69	75	50	90	91
	2	28	75	82	63	95	86
	ref	20	29	53	61	100	100
	1	58	40	50	100	100	94
	2	45	46	49	100	100	85
	ref	72	73	62	100	100	100
	1	84	46	79	55	78	72
	2	76	20	77	63	84	79
	ref	84	42	86	95	94	92

When comparing the activity and selectivity of the PSP-based complexes **1** and **2** with the dppe analogue [NiBr₂(dppe)], a drop in selectivity, especially in coordinating solvent, occurs, which might stem from the lability of the PSP ligand based on the higher ring strain within the four-membered Ni–P–S–P ring compared to the five-membered ring in the dppe analogue. Thus, a

higher number of off-pathway reactions causes the formation of side products, mainly homocoupling products of the Grignard reagents. However, one big advantage of the PSP-based nickel complexes compared to $[\text{NiBr}_2(\text{dppe})]$ can be found in the coupling of sterically more demanding Grignard reagents, such as MesMgBr . Whereas with **2** 82% conversion of 2-bromopyridine and MesMgBr can be achieved in toluene, only 53% conversion were observed when the reference catalyst in toluene was applied. In this case, the more dynamic coordination sphere around the Ni-centre in the PSP-containing complexes, appears to enhance the catalytic conversion. In the context of new drug developments, recent research focuses on establishing alternative pathways of $\text{C}(sp^2)\text{--C}(sp^3)$ couplings.^{26,27} Major obstacles affecting these conversions include side-reactions, such as homocouplings or competing β -hydride eliminations.^{28,29} As part of this study, the coupling reactions of bromobenzene or -pyridine with cyclohexyl magnesium bromide were investigated. Hereby, the use of PSP catalysts has led to similar results, as the application of the dppe-based reference catalyst (Table S3).

Conclusions

In conclusion, we report the synthesis of two PSP-stabilised nickel halide complexes, namely $[\text{NiHal}_2(\text{PSP})]$, $\text{PSP} = \text{Ph}_2\text{PSPPh}_2$, $\text{Hal} = \text{Br}$ (**1**), I (**2**), where the incorporation of sulphur into the ligand backbone drastically influences the compounds molecular structure, spectroscopic (UV/Vis, IR and NMR) properties as well as their catalytic performance compared to the PCP analogues. While bromide and iodide complexes, of the form, could be successfully isolated, the conversion of NiCl_2 with PPS leads to the isolation of an interesting multinuclear nickel complex **3** through rearrangement reactions of the parent PSP ligand. Multinuclear complexes, such as **4** and **5**, could also be obtained from the reaction of $[\text{Ni}(\text{COD})_2]$ with the ligand or its precursor compounds (KPS and ClPPh_2). During these reactions the oxidation of $\text{Ni}(0)$ to $\text{Ni}(\text{II})$ is observed.

To investigate the so far unexplored application of the PSP ligand, a sulphur analogue of the widely applied PCP-type ligands, in catalysis, [NiHal₂(PSP)] (Hal = Br, I) complexes were successfully used as catalysts in Kumada-Tamao-Corriu couplings of aryl halides and aromatic Grignard reagents. Hereby no evidence of catalyst poisoning through the sulphur-containing ligand backbone was observed and PSP-based nickel(II) complexes show promising catalytic performance, especially for the conversion of sterically demanding reagents. A strong impact of the solvent came to light with PSP- and dppe-based nickel complexes as well as a drop in selectivity with the PSP-stabilised Ni-complexes compared to the dppe analogues. This might stem from off-pathway reactions due to dynamic ligand behaviour of the PSP ligand. The suppression of these side reactions *via* a targeted modification of the residues of the PSP scaffold is currently being investigated.

Experimental Section

Materials, Methods and Instruments

All experiments were carried out under Ar-atmosphere using Schlenk-techniques and an Ar-filled glove box (MBraun). Toluene, tetrahydrofuran (THF), *n*-pentane and *n*-heptane were dried using a solvent purification system (MBraun SPS-800) and degassed before use. THF was further distilled over potassium/benzophenone. Acetonitrile (MeCN) and dichloromethane (DCM) were distilled over CaH₂. Deuterated solvents were dried over P₂O₅ (CDCl₃ and CD₂Cl₂) or over CaH₂ (C₆D₆, D₈-toluene and CD₃CN). Before use, deuterated solvents were degassed through three freeze-pump-thaw cycles and stored over molecular sieves (MeCN and CD₃CN over 3 Å, all other over 4 Å). NMR spectra were recorded on Bruker Avance III or Avance Neo 400 MHz spectrometers at 298 K. Chemical shifts are described in parts per million (ppm) and are referenced to residual solvent signals of the deuterated solvents. For the distinct assignment of the signals,

chemical shifts, coupling patterns and 2D experiments (^1H - ^1H COSY, ^1H - ^{13}C HMQC, ^1H - ^{13}C HMBC) are used. Multiplicities of the NMR signals are abbreviated as s = singlet, d = doublet, t = triplet, dd = doublet of doublets, ddd = doublet of doublets of doublets, dt = doublet of triplets, m = multiplet, br = broad. The NMR data was processed using MestreNova. Infrared (IR) spectra were conducted using a Bruker Tensor 37 FTIR spectrometer equipped with a room-temperature DLaTGS detector, a diamond ATR (attenuated total reflection) unit, and a nitrogen-flushed measurement chamber in the region of 4000–450 cm^{-1} . Signals were divided into vs = very strong, s = strong, m = medium, w = weak and vw = very weak. Data was processed with the program Origin. Single crystals were measured on a STOE STADIVARI and on a STOE METAL JET D2 diffractometer. The STOE STADIVARI is equipped with an open Eulerian cradle (4-circle) and a DECTRIS PILATUS pixel detector at 100 K with a microfocus molybdenum source (Mo-K α , $\lambda = 0.71073 \text{ \AA}$) using a graphite monochromator as radiation source. The STOE METAL JET 2D contains a EIGER4M Detector with a sealed X-Ray tube (Mo-K α , $\lambda = 0.71073 \text{ \AA}$) and a graded multilayer mirror monochromator. A liquid-gallium-jet anode is utilized as radiation source. The data reduction was conducted with X-Area version 1.73.1.0 (STOE, 2018)³⁰ using the semi-empirical absorption correction by X-RED with scaling of the reflection intensities by LANA included in X-Area. Structures were solved by means of dual space methods with SHELXT-2015³¹ and refinement was performed with SHELXL-2018³² using the WinGX³³ program suite. Full-matrix least-square routines against F^2 were carried out. Hydrogen atoms were calculated on idealized positions. Pictures were generated with the program DIAMOND³⁴. For these thermal ellipsoids are shown with 30% probability and hydrogen atoms as well as co-crystallised solvent molecules are omitted for clarity. CCDC 2375582 (**1**), CCDC 2375583 (**2**), CCDC 2375585 (**3**), CCDC 2375584 (**4**), and CCDC 2375581 (**5**) contain the supplementary crystallographic data for

this paper. These data can and additional information can be obtained free of charge *via* <https://summary.ccdc.cam.ac.uk/structure-summary-form> (or from the Cambridge Crystallographic Data Centre, 12 Union Road, Cambridge CB2 1EZ, UK; fax: (+44)1223-336-033; or deposit@ccdc.cam.ac.uk). UV/Vis spectra were recorded using an Ocean FX UV-Vis spectrometer from Ocean Optics. Therefore, solutions with a concentration of $c = 1 \cdot 10^{-4} \text{ mol L}^{-1}$ were prepared. Data was processed with the program Origin. Elemental analysis of the samples was conducted with a vario EL cube or a vario MICRO cube (Elementar Analysensysteme GmbH). Catalytic tests were qualitatively and quantitatively evaluated by means of GC-MS using an Agilent 8860 GC and a 5977B MSD whereby *n*-decane was used as internal standard.

Syntheses

Tetraphenyl diphosphine sulphide ($\text{Ph}_2\text{P}(=\text{S})\text{-PPh}_2$, PPS)

PPS was prepared by dissolving diphenyl phosphine sulphide (1 g, 4.582 mmol, 1 eq.) in toluene, adding triethylamine (0.61 g, 0.83 mL, 1.3 eq.) and cooling with an ice bath to 0-5°C. Chlorodiphenylphosphine (1.03 g, 0.84 mL, 4.582 mmol, 1 eq.) diluted in toluene, was added slowly to the solution of diphenyl phosphine sulphide. After stirring overnight, the solution was filtered and the solvent was partially evaporated *in vacuo*. The solution was cooled to -30°C and overnight colorless crystals were grown. The crystals were washed with *n*-pentane and dried *in vacuo* (0.977 g, crystalline yield: 53.0 %).

^1H NMR (298 K, CDCl_3 , 400 MHz), δ [ppm] = 8.14 (m, 4 H), 7.71 (m, 4 H), 6.95 (m, 12 H)

$^{31}\text{P}\{^1\text{H}\}$ NMR (298 K, CD_2Cl_2 , 162 MHz), δ [ppm] = 44.3 (d, P=S, $^2J_{\text{PP}} = 247.3 \text{ Hz}$), -13.8 (d, PPh_2 , $^2J_{\text{PP}} = 247.3 \text{ Hz}$)

[NiBr₂(PSP)] (1)

NiBr₂ (100.0 mg, 0.46 mmol, 1 eq.) was heated to reflux with the PPS (Ph₂P(=S)–PPh₂; 184.2 mg, 0.46 mmol, 1 eq.) ligand in acetonitrile (6 mL) for 5 hours. The reaction mixture was filtered, and the solvent was subsequently removed *in vacuo*. Through redissolving the solid residue in DCM and layering with *n*-heptane, 139.8 mg of compound **1** in 49.2% crystalline yield were obtained.

¹H NMR (298 K, CD₂Cl₂, 400 MHz), δ [ppm] = 8.11 (m, 8 H, Ph-H-*ortho*), 7.66 (t, 4 H, $J_{\text{HH}} = 7.6$ Hz, Ph-H-*para*); 7.56 (t, 8 H, $J_{\text{HH}} = 7.6$ Hz, Ph-H-*meta*)

³¹P{¹H} NMR (298 K, CD₂Cl₂, 162 MHz), δ [ppm] = –17.5 (s)

¹³C NMR (298 K, CD₂Cl₂, 101 MHz), δ [ppm] = 134.0 (br, Ar-C-*ortho*), 133.1 (s, Ar-C-*para*), 129.5 (br, Ar-C-*meta*)

ATR-IR (cm⁻¹): $\tilde{\nu} = 1478$ (w), 1431(m), 1382(vw), 1330 (vw), 1305 (vw), 1182 (w), 1161 (vw), 1139 (vw), 1088 (m), 1066 (w), 1022 (vw), 995 (w), 970 (vw), 921 (vw), 838 (vw), 754 (w), 740 (s), 710 (w), 694 (m), 682 (vs), 617 (vw), 561 (vs), 534 (w), 507 (vs), 474 (w), 468 (vs), 459 (s), 434 (m)

UV/Vis [dcm, nm (mol⁻¹dm³cm⁻¹): λ_{max} (ϵ) = 510 (2391), 304 (17069), 277 (21175), 255 (24981)

Elemental analysis calculated (%) for C₂₄H₂₀Br₂NiP₂S · 0.5 DCM: C 44.36, H 3.19, S 4.83 found: C 44.36, H 3.26, S 4.88

[NiI₂(PSP)] (2)

NiI₂ (100.0 mg, 0.32 mmol, 1 eq.) and PPS (128.8 mg, 0.32 mmol, 1 eq.) were brought to reflux in acetonitrile (6 mL) for 5 hours. The reaction mixture was filtered. After removing the solvent *in vacuo*, redissolving the resulting solid residue in DCM and layering with *n*-heptane, 105.7 mg of single-crystals were obtained in 46.2 % crystalline yield.

^1H NMR (298 K, CD_2Cl_2 , 400 MHz), δ [ppm] = 8.10 (m, 8 H, Ph-H-*ortho*), 7.64 (t, 4 H, $J_{\text{HH}} = 7.5$ Hz, Ph-H-*para*); 7.56 (t, 8 H, $J_{\text{HH}} = 7.5$ Hz, Ph-H-*meta*)

$^{31}\text{P}\{^1\text{H}\}$ NMR (298 K, CD_2Cl_2 , 162 MHz), δ [ppm] = -14.5 (s)

^{13}C NMR (298 K, CD_2Cl_2 , 101 MHz), δ [ppm] = 134.3 (m, Ar-C-*ortho*), 132.9 (s, Ar-C-*para*), 129.3 (m, Ar-C-*meta*)

ATR-IR (cm^{-1}): $\tilde{\nu} = 1478$ (w), 1431 (m), 1383 (vw), 1330 (vw), 1303 (vw), 1178 (w), 1161 (vw), 1141 (vw), 1088 (m), 1066 (vw), 1022 (vw), 995 (w), 970 (vw), 923 (vw), 835 (vw), 754 (w), 739 (s), 710 (w), 694 (m), 685 (vs), 615 (vw), 557 (vs), 528 (m), 505 (vs), 474 (w), 464 (s), 453 (s), 434 (m)

UV/Vis (dcm, nm [$\text{mol}^{-1}\text{dm}^3\text{cm}^{-1}$]): λ_{max} (ϵ) = 564 (2297), 387 (3347), 303 (18242), 250 (24786)

Elemental analysis calculated (%) for $\text{C}_{24}\text{H}_{20}\text{I}_2\text{NiP}_2\text{S}$: C 40.32, H 2.82, S 4.48 found: C 40.22, H 3.03, S 4.00

[Ni₂(Ph₂PSS)₂(Ph₂PS)(Ph₂P)] (3)

3 was obtained through the conversion of NiCl_2 (70.0 mg, 0.54 mmol, 1 eq.) and PPS (217.3 mg, 0.54 mmol, 1 eq.) under reflux conditions in acetonitrile (6 mL). After 5 h of reaction, the mixture was filtered and the solvent evaporated *in vacuo*. 17.0 mg of dark-brown crystals suitable for SXRD were obtained by dissolving the solid residue in DCM and layering the solution with *n*-pentane in a crystalline yield of 6 %.

^1H NMR (298 K, CD_2Cl_2 , 400 MHz), δ [ppm] = 8.06–7.93 (m, 8 H, *o*-Ph₂PSS⁻), 7.70–7.64 (m, 2 H, *p*-Ph₂PS⁻), 7.64–7.58 (m, 4 H, *o*-Ph₂P⁻), 7.58–7.54 (m, 2 H, *p*-Ph₂P⁻), 7.54–7.48 (m, 4 H, *m*-Ph₂P⁻), 7.48–7.41 (m, 8 H, *o,m*-Ph₂PS⁻), 7.41–7.28 (m, 8 H, *m*-Ph₂PSS⁻), 7.27–7.18 (m, 4 H, *p*-Ph₂PSS⁻)

$^{31}\text{P}\{^1\text{H}\}$ NMR (298 K, CD_2Cl_2 , 162 MHz), δ [ppm] = 92.0 (dt, 1 P_b , Ph_2PS^- , $^2J_{\text{PP}} = 49.0$ Hz, $^3J_{\text{PP}} = 3.6$ Hz), 72.7 (s, 1 P_d , Ph_2PSS^-), 72.0 (t, 1 P_a , Ph_2PSS^- , $^3J_{\text{PP}} = 3.6$ Hz), 60.4 (dd, 1 P_c , Ph_2P^- , $^2J_{\text{PP}} = 49.0$ Hz, $^3J_{\text{PP}} = 3.6$ Hz)

^{13}C NMR (298 K, CD_2Cl_2 , 101 MHz), δ [ppm] = 135.8, 134.5 (d), 132.8 (d), 131.9 (dd), 130.1 (br), 129.8 (dd), 128.5 (dd), 128.5 (s), 128.0 (d), 127.4 (d)

ATR-IR (cm^{-1}): $\tilde{\nu} = 3043$ (vw), 1961 (vw), 1877 (vw), 1810 (w), 1774 (w), 1697 (w), 1653 (w), 1616 (vw), 1577 (w), 1561 (w), 1540 (w), 1523 (vw), 1508 (vw), 1475 (m), 1432 (m), 1395 (w), 1328 (w), 1305 (m), 1264 (w), 1179 (m), 1158 (w), 1094 (s), 1067 (m), 1026 (m), 994 (m), 972 (w), 920 (w), 847 (w), 741 (s), 706 (s), 687 (vs), 628 (m), 607 (m), 571 (vs), 520 (m), 488 (s), 475 (s)

Elemental analysis calculated (%) for $\text{C}_{48}\text{H}_{40}\text{Ni}_2\text{P}_4\text{S}_5$: C 56.61, H 3.96, S 15.74 found: C 56.24, H 4.03, S 15.97

$[\text{Ni}_3(\text{Ph}_2\text{PS})_4(\text{Ph}_2\text{P})_2]$ (4)

$[\text{Ni}(\text{COD})_2]$ (50.0 mg, 0.18 mmol, 1 eq.) was reacted with PPS (146.3 mg, 0.36 mmol, 2 eq.) in DCM (6 mL) at room temperature. After stirring overnight, the reaction solution was filtered and layered with *n*-pentane. After 2 days, dark red crystals suitable for single crystal XRD were obtained in 27 % crystalline yield (23.2 mg).

^1H NMR (298 K, CDCl_3 , 400 MHz), δ [ppm] = 8.00–7.73 (m, 4 H, $p\text{-Ph}_2\text{PS}^-_{\text{intern}}$), 7.72–7.57 (m, 4 H, $p\text{-Ph}_2\text{P}^-$), 7.56–7.44 (m, 4 H, $p\text{-Ph}_2\text{PS}^-_{\text{terminal}}$), 7.42–7.27 (m, 8 H, $o\text{-Ph}_2\text{PS}^-_{\text{intern}}$), 7.28–6.78 (m, 40 H: 8 H $m\text{-Ph}_2\text{PS}^-_{\text{intern}}$, 8 H $m\text{-Ph}_2\text{P}^-$, 8 H $o\text{-Ph}_2\text{P}^-$, 8 H $m\text{-Ph}_2\text{PS}^-_{\text{terminal}}$, 8 H $o\text{-Ph}_2\text{PS}^-_{\text{terminal}}$)

$^{31}\text{P}\{^1\text{H}\}$ NMR (298 K, CDCl_3 , 162 MHz), δ [ppm] = 98.1 (br, 2 P_c , $\text{Ph}_2\text{PS}^-_{\text{intern}}$), 41.4 (br, 2 P_b , Ph_2P^-), 30.0 (br, 1 P_a , $\text{Ph}_2\text{PS}^-_{\text{terminal}}$), 23.2 (2 m, 1 P_a , $\text{Ph}_2\text{PS}^-_{\text{terminal}}$)

^{13}C NMR (298 K, CDCl_3 , 101 MHz), δ [ppm] = 135.0 (br), 133.9 (br), 133.1–132.3 (br), 128.5 (br), 128.4 (br), 127.1 (br)

ATR-IR (cm^{-1}): $\tilde{\nu}$ = 3068 (w), 3049 (w), 1953 (vw), 1882 (vw), 1805 (w), 1772 (vw), 1699 (w), 1650 (w), 1616 (w), 1580 (w), 1558 (w), 1539 (w), 1520 (vw), 1506 (vw), 1475 (m), 1432 (s), 1395 (w), 1323 (w), 1304 (m), 1267 (m), 1243 (m), 1182 (m), 1155 (m), 1128 (m), 1089 (s), 1066 (m), 1026 (m), 997 (m), 968 (w), 918 (w), 844 (w), 736 (s), 687 (vs), 617 (m), 582 (m), 557 (s), 516 (m), 498 (s), 486 (vs), 473 (s)

Elemental analysis calculated (%) for $\text{C}_{72}\text{H}_{60}\text{Ni}_3\text{P}_6\text{S}_4$: C 61.1, H 4.27, S 9.06 found: C 60.63, H 4.40, S 8.51

[Ni₂(Ph₂PSS)(Ph₂PS)₂(Ph₂P)] (5)

[Ni(COD)₂] (50.0 mg, 0.18 mmol, 1 eq.) and KPPH₂ (93.2 mg, 0.36 mmol, 2 eq.) were dissolved in toluene (6 mL) at room temperature. ClPPH₂ (80.2 mg, 67 μL , 0.36 mmol, 2 eq.) was added and stirred overnight. The reaction mixture was filtered and layered with *n*-pentane affording dark brown crystals in 15 % crystalline yield (13.3 mg).

^1H NMR (298 K, CD_2Cl_2 , 400 MHz), δ [ppm] = 8.08–7.97 (m, 4 H, *o*-Ph₂PSS⁻), 7.68–7.57 (m, 4 H, *o*-Ph₂PS⁻_{intern}), 7.57–7.35 (m, 18 H: 4 H, *m*-Ph₂PSS⁻, 2 H, *p*-Ph₂PSS⁻, 4 H, *m*-Ph₂PS⁻_{intern}, 2 H, *p*-Ph₂PSS⁻, 2 H, *p*-Ph₂P⁻, 4 H, *m*-Ph₂PS⁻_{terminal}) 7.30–7.18 (m, 4 H, *o*-Ph₂PS⁻_{terminal}), 7.18–7.09 (m, 4 H, *m*-Ph₂P⁻), 7.03–6.96 (m, 2 H, *p*-Ph₂PS⁻_{terminal}), 6.96–6.85 (m, 4 H, *o*-Ph₂P⁻)

$^{31}\text{P}\{^1\text{H}\}$ NMR (298 K, CD_2Cl_2 , 162 MHz), δ [ppm] = 90.1 (ddd, 1 P_b, Ph₂PS⁻_{intern}, $^2J_{\text{PP}} = 42.9$ Hz, $^3J_{\text{PP}} = 6.7$ Hz, $^3J_{\text{PP}} = 3.3$ Hz), 73.0 (t, 1 P_a, Ph₂PSS⁻, $^3J_{\text{PP}} = 3.3$ Hz), 56.3 (ddd, 1 P_c, Ph₂P⁻, $^2J_{\text{PP}} = 42.9$ Hz, $^2J_{\text{PP}} = 31.0$ Hz, $^3J_{\text{PP}} = 3.3$ Hz), 31.0 (dd, 1 P_d, Ph₂PS⁻_{terminal}, $^2J_{\text{PP}} = 31.0$ Hz, $^3J_{\text{PP}} = 6.7$ Hz)

^{13}C NMR (298 K, CD_2Cl_2 , 101 MHz), δ [ppm] = 134.3 (d), 133.4–133.0 (m), 132.2 (br), 131.2 (br), 130.2 (d), 128.8 (t), 128.7 (br), 128.4 (br), 127.7 (br), 127.6 (br)

ATR-IR (cm^{-1}): $\tilde{\nu} = 3068$ (vw), 3049 (vw), 1801 (vw), 1770 (vw), 1699 (vw), 1681 (vw), 1648 (vw), 1581 (w), 1558 (vw), 1539 (vw), 1523 (vw), 1506 (vw), 1475 (w), 1433 (m), 1389 (vw), 1327 (vw), 1306 (w), 1273 (vw), 1182 (w), 1157 (w), 1093 (m), 1068 (w), 1026 (w), 997 (w), 970 (vw), 919 (vw), 847 (vw), 741 (s), 689 (vs), 635 (vw), 619 (vw), 577 (m), 559 (s), 517 (m), 488 (vs)

Elemental analysis calculated (%) for $\text{C}_{48}\text{H}_{40}\text{Ni}_2\text{P}_4\text{S}_4 \cdot 0.7$ toluene: C 60.46, H 4.37, S 12.2 found: C 60.45, H 4.81, S 11.76

Catalytic tests

All catalytic tests have been conducted under Argon atmosphere in Young-NMR tubes at room temperature for 20 h if not noted otherwise. All catalytic tests were conducted with **1**, **2** and in parallel with the reference catalyst $[\text{NiBr}_2(\text{dppe})]$. The substrates (aryl halide, 0.1 mmol) and Grignard reagent (1.0 eq., 0.1 mmol), catalyst (5.0 mol%), and the internal standard *n*-decane (20 μL) have been dissolved in 0.5 mL of solvent (either THF, benzene or toluene). For $\text{C}(sp^2)\text{-C}(sp^3)$ coupling, the quantity of the catalysts was increased to 10 mol%. During the addition of the reagents, the mixture was cooled down to $0\text{--}5^\circ\text{C}$ and the mixture was allowed to slowly warm to room temperature overnight. After completion of the reaction time, the reaction mixture was filtered and analysed by GC-MS (100 μL sample in 1 mL EtOH).

ACKNOWLEDGMENT

The authors wish to thank the Stiftung der Deutschen Wirtschaft for a doctoral scholarship for F.F. We wish to thank Prof. Dieter Fenske for his continuous support with single crystal XRD measurements. Further we would like to thank Nhu Phong Nguyen and Lorena Damsch for their experimental help.

REFERENCES

- (1) Chernyshev, V. M.; Ananikov, V. P. Nickel and Palladium Catalysis: Stronger Demand than Ever. *ACS Catal.* **2022**, *12* (2), 1180-1200. DOI: 10.1021/acscatal.1c04705.
- (2) Cooper, A. K.; Burton, P. M.; Nelson, D. J. Nickel versus Palladium in Cross-Coupling Catalysis: On the Role of Substrate Coordination to Zerovalent Metal Complexes. *Synth.* **2020**, *52* (04), 565-573. DOI: 10.1055/s-0039-1690045.
- (3) Ananikov, V. P. Nickel: The “Spirited Horse” of Transition Metal Catalysis. *ACS Catal.* **2015**, *5* (3), 1964-1971. DOI: 10.1021/acscatal.5b00072.
- (4) Han, F.-S. Transition-metal-catalyzed Suzuki–Miyaura cross-coupling reactions: a remarkable advance from palladium to nickel catalysts. *Chem. Soc. Rev.* **2013**, *42* (12), 5270-5298. DOI: 10.1039/C3CS35521G.
- (5) Kumada, M. Nickel and palladium complex catalyzed cross-coupling reactions of organometallic reagents with organic halides. *Pure Appl. Chem.* **1980**, *52* (3), 669-679. DOI: 10.1351/pac198052030669.
- (6) Tamao, K.; Sumitani, K.; Kumada, M. Selective carbon-carbon bond formation by cross-coupling of Grignard reagents with organic halides. Catalysis by nickel-phosphine complexes. *J. Am. Chem. Soc.* **1972**, *94* (12), 4374-4376. DOI: 10.1021/ja00767.
- (7) Yamamoto, Y.; Fujiwara, K.; Ogawa, A. Palladium-Catalyzed Hydrophosphination of Terminal Alkynes with Diphenylphosphine Oxide in the Presence of Tetraphenyldiphosphine Monoxide. *Organometallics* **2023**, *42* (18), 2590-2597. DOI: 10.1021/acs.organomet.2c00659.
- (8) Li, G. Y.; Marshall, W. J. Air-Stable Phosphine Sulfide Ligand Precursors for Nickel-Catalyzed Cross-Coupling Reactions of Unactivated Aryl Chlorides with Aryl Grignard Reagents. *Organometallics* **2002**, *21* (4), 590-591. DOI: 10.1021/om010828.
- (9) Yogendra, S.; Chitnis, S. S.; Hengersdorf, F.; Bodensteiner, M.; Fischer, R.; Burford, N.; Weigand, J. J. Condensation Reactions of Chlorophosphanes with Chalcogenides. *Inorg. Chem.* **2016**, *55* (4), 1854-1860. DOI: 10.1021/acs.inorgchem.5b02723.
- (10) Flecken, F.; Knapp, A.; Grell, T.; Dreßler, C.; Hanf, S. Acute Bite Angle POP- and PSP-Type Ligands and Their Trinuclear Copper(I) Complexes: Synthesis and Photo-Luminescence Properties. *Inorg. Chem.* **2023**, *62* (32), 13038-13049. DOI: 10.1021/acs.inorgchem.3c01865.
- (11) Cotton, F. A.; Falvello, L. R.; Tomas, M.; Gray, G. M.; Krainhanzel, C. S. Molybdenum carbonyl complexes of diphenylphosphinous acid and diphenylphosphinous acid derivatives. Crystal and molecular structures of [Et₄N][Mo(CO)₄(PPh₂O)₂H]·0.37 CH₂Cl₂, Mo(CO)₄(PPh₂OH)(PPh₂OCH₂CH₂NMe₂)·H₂O and Mo(CO)₄(PPh₂SPPh₂). *Inorg. Chim. Acta* **1984**, *82* (2), 129-139. DOI: 10.1016/S0020-1693(00)82481-0.
- (12) Sues, P. E.; Lough, A. J.; Morris, R. H. A sulfur mimic of 1,1-bis(diphenylphosphino)methane: a new ligand opens up. *Chem. Commun.* **2014**, *50* (36), 4707-4710. DOI: 10.1039/C3CC49456J.
- (13) Jones, P. G.; Fischer, A. K.; Farkens, M.; Schmutzler, R. Penta-carbonyl-(tetra-phenyl-diphosphine mono-sulfide-P)-chromium(0). *Acta. Cryst. E* **2002**, *58* (9), m478-m479. DOI: 10.1107/S1600536802014125.
- (14) Einspahr, H.; Donohue, J. Crystal and molecular structure of .mu.-carbonyl-bis-.mu.-[bis(bis(trifluoromethyl)phosphino)sulfur-P,P']-bis(carbonylnickel). *Inorg. Chem.* **1974**, *13* (8), 1839-1843. DOI: 10.1021/ic50138.

- (15) Duffy, M. P.; Lin, Y.; Ting, L. Y.; Mathey, F. Intramolecular [4+2] versus [2+2] cycloadditions in P–X–P-linked biphospholes (X = O, S). *New J. Chem.* **2011**, *35* (10), 2001-2003. DOI: 10.1039/C1NJ20087A.
- (16) Hoehne, S.; Lindner, E.; Gumz, J.-P. Das Verhalten von Mono- und Diorganylphosphinsulfiden gegenüber Metallcarbonylsystemen, XIX: Die Stabilisierung von Dithiobis(dimethylphosphin), [(CH₃)₂PS-]₂. Kristall- und Molekülstrukturen von [η⁵-C₅H₅(OC)₂MnP(CH₃)₂S-]₂ und [η⁵-C₅H₅(OC)₂MnP(CH₃)₂]₂S. *Chem. Ber.* **1978**, *111* (12), 3818-3822. DOI: 10.1002/cber.19781111207.
- (17) Okuniewski, A.; Rosiak, D.; Chojnacki, J.; Becker, B. Coordination polymers and molecular structures among complexes of mercury(II) halides with selected 1-benzoylthioureas. *Polyhedron* **2015**, *90*, 47-57. DOI: 10.1016/j.poly.2015.01.035.
- (18) Lomjanský, D.; Rajnák, C.; Titiš, J.; Moncol, J.; Smolko, L.; Boča, R. Impact of tetrahedral and square planar geometry of Ni(II) complexes with (pseudo)halide ligands to magnetic properties. *Inorg. Chim. Acta* **2018**, *483*, 352-358. DOI: 10.1016/j.ica.2018.08.029.
- (19) Puddephatt, R. J. Chemistry of bis(diphenylphosphino)methane. *Chem. Soc. Rev.* **1983**, *12* (2), 99-127. DOI: 10.1039/CS9831200099.
- (20) Rahn, J. A.; Delian, A.; Nelson, J. H. Unanticipated formation of dibromo[1,2-bis(diphenylphosphino)ethane]nickel(II) by sequential Michael reversion and Michael addition of dibromobis(diphenylvinylphosphine)nickel(II). *Inorg. Chem.* **1989**, *28* (2), 215-217. DOI: 10.1021/ic00301.
- (21) Fergusson, J. E.; Heveltdt, P. F. Tertiary phosphine complexes of nickel, palladium, platinum, cobalt and zinc: a spectroscopic study. *Inorg. Chim. Acta* **1978**, *31*, 145-154. DOI: 10.1016/S0020-1693(00)94992-2.
- (22) Sato, Y.; Kawaguchi, S.-i.; Nomoto, A.; Ogawa, A. Synthesis of Bis(phosphanyl)alkane Monosulfides by the Addition of Diphosphane Monosulfides to Alkenes under Light. *Chem. Eur. J* **2018**, *25* (9), 2295-2302. DOI: 10.1002/chem.201805114.
- (23) Yamamoto, Y.; Tanaka, R.; Ota, M.; Nishimura, M.; Tran, C. C.; Kawaguchi, S.-i.; Kodama, S.; Nomoto, A.; Ogawa, A. Photoinduced Syntheses and Reactivities of Phosphorus-Containing Interelement Compounds. *J. Org. Chem.* **2020**, *85* (22), 14708-14719. DOI: 10.1021/acs.joc.0c02014.
- (24) Yamamoto, Y.; Ogawa, A. Photoinduced Synthesis of Bisphosphinated Quinoxalines via Radical Cyclization of o-Diisocyanoarenes with Diphosphines. *Chem. Asian J.* **2023**, *18* (8), e202201269. DOI: 10.1002/asia.202201269.
- (25) Tamao, K. Discovery of the cross-coupling reaction between Grignard reagents and C(sp²) halides catalyzed by nickel–phosphine complexes. *J. Organomet. Chem.* **2002**, *653* (1-2), 23-26. DOI: 10.1016/S0022-328X(02)01159-2.
- (26) Dombrowski, A. W.; Gesmundo, N. J.; Aguirre, A. L.; Sarris, K. A.; Young, J. M.; Bogdan, A. R.; Martin, M. C.; Gedeon, S.; Wang, Y. Expanding the Medicinal Chemist Toolbox: Comparing Seven C(sp²)–C(sp³) Cross-Coupling Methods by Library Synthesis. *ACS Med. Chem. Lett.* **2020**, *11* (4), 597-604. DOI: 10.1021/acsmchemlett.0c00093.
- (27) Palaychuk, N.; DeLano, T. J.; Boyd, M. J.; Green, J.; Bandarage, U. K. Synthesis of Cycloalkyl Substituted 7-Azaindoles via Photoredox Nickel Dual Catalytic Cross-Coupling in Batch and Continuous Flow. *Org. Lett.* **2016**, *18* (23), 6180-6183. DOI: 10.1021/acs.orglett.6b03223.

- (28) Jana, R.; Pathak, T. P.; Sigman, M. S. Advances in Transition Metal (Pd,Ni,Fe)-Catalyzed Cross-Coupling Reactions Using Alkyl-organometallics as Reaction Partners. *Chem. Rev.* **2011**, *111* (3), 1417-1492. DOI: 10.1021/cr100327.
- (29) Piontek, A.; Ocheźdzan-Siodłak, W.; Bisz, E.; Szostak, M. Nickel-Catalyzed C(sp²)-C(sp³) Kumada Cross-Coupling of Aryl Tosylates with Alkyl Grignard Reagents. *Adv. Synth. Catal.* **2019**, *361* (10), 2329-2336. DOI: 10.1002/adsc.201801586.
- (30) *X-RED, Program for data reduction and absorption correction*; Stoe & Cie GmbH: Darmstadt, Germany, 2005. (accessed.
- (31) Sheldrick, G. M. SHELXT – Integrated space-group and crystal-structure determination. *Acta. Cryst. A* **2015**, *71* (1), 3-8. DOI: 10.1107/S2053273314026370.
- (32) Sheldrick, G. M. Crystal structure refinement with SHELXL. *Acta. Cryst. B* **2015**, *71* (Pt 1), 3-8. DOI: 10.1107/S2053229614024218.
- (33) Farrugia, L. J. WinGX and ORTEP for Windows: an update. *J. Appl. Crystallogr.* **2012**, *45* (4), 849-854. DOI: 10.1107/S0021889812029111.
- (34) *Diamond - Crystal and Molecular Structure Visualization*; Crystal Impact: Bonn, Germany, 1999. (accessed 13.07.2024).